
Fracture 1977, Volume 2, ICF4, Waterloo, Canada, June 19 - 24, 1977

STRUCTURAL DAMAGE IN SHEET METAL FORMING

Gustau Ferran and Sergio Leite de Andrade*

INTRODUCTION

Deformation processing of sheet metal encompasses different states of plane stress, extending from tension-compression ($\varepsilon_{p_1} > 0 > \varepsilon_{p_2}$), through plane strain ($\varepsilon_{p_1} > 0 = \varepsilon_{p_2}$), to balanced biaxial tension ($\varepsilon_{p_1} = \varepsilon_{p_2} > 0$). Forming Limit Curves (FLC) [1] describing the maximum strains that sheet metal can withstand before failure have been of great practical use in the press shop; however the physical processes leading to failure are not well understood, especially between $\varepsilon_{p_2} = 0$ and $\varepsilon_{p_1} = \varepsilon_{p_2} > 0$. Ghosh and Hecker [2] proposed a new model of failure in thin sheets, based upon geometrical and frictional constraints that finally satisfy an instability condition and reach a state of strain localization. This rationalization of localized necking does not require a pre-existing trough, as does the model proposed by Marciniak and Kuczynski [3], and does not take into account the inclusions in the metal. Although there is a large amount of information available concerning the different states of stress and strain, there is a lack of published information concerning the damage introduced during sheet forming [4, 5]. Considering that such information may be relevant to a better understanding of the mechanism leading to failure, a research programme was started on the subject. This paper deals first with the morphology of the damage introduced by sheet forming, observed with the scanning electron microscope. Secondly, some quantitative results on the damage introduced by balanced biaxial stress are described.

EXPERIMENTAL METHODS

Tests were carried out on a low carbon rimmed steel sheet, 1.23 mm thick, of drawing quality, with chemical composition: $|C| = 0.06\%$ $|Mn| = 0.28\%$ $|P| = 0.008\%$ $|S| = 0.016\%$ and the following mechanical properties: Yield Strength: 233 MPa, Ultimate Tensile Strength: 313 MPa, Strain Hardening Exponent: $\bar{n} = 0.187$, $\bar{n} = |n(0^\circ) + n(90^\circ) + 2n(45^\circ)|/4$, Plastic Anisotropy coefficient: $\bar{r} = 1.23$, $\bar{r} = |r(0^\circ) + r(90^\circ) + 2r(45^\circ)|/4$. Where 0°, 90°, 45°, represent the angle between the direction of the uniaxial tension test and the rolling direction.

The symmetrical expansion ($\varepsilon_{p_1} = \varepsilon_{p_2} > 0$) test was carried out on a very simple punch-matrix attachment, fitted to a hydraulic press [6]. The radius of the hemispherical punch, 50 mm, and the other main geometrical characteristics of the attachment were similar to the ones described by Veerman [7]. This test was conducted on square blanks of 190 mm side, using a soft rubber sheet 10 mm thick as lubricant. The punch was moving at a constant speed of 0.4 mm/min. The test blanks were photoprinted with 5.0 mm diameter circles using a photosensitive resist process. Measurements of the instantaneous strains, (ε_{p_1}, ε_{p_2}), were made along a radial

---

* Metalurgia COPPE/UFRJ, Caixa Postal 1191 ZC-00, 20.000, Rio de Janeiro, RJ, Brazil

direction, interrupting the test 13 times before failure.

The fractured samples and a non-deformed sample, as a basis for comparison, were examined metallographically on sections parallel and perpendicular to the rolling plane. Sections parallel to the rolling plane, prepared by mechanical polishing and finishing with alumina, were observed optically, and also in a scanning electron microscope. The quantitative measurements were all made at 800 magnifications, and in the Stereoscan at 2600 magnifications. Since the surfaces observed contained usually three features (inclusions, cavities and microcracks), with different shapes (extending from circles to very narrow rectangles), areal analysis was considered more convenient to represent the size distribution. The area of each feature was estimated as the product $\underline{a_1}$ times $\underline{a_2}$, where $\underline{a_1}$ and $\underline{a_2}$ were the two maximum dimensions measured directly on the microscope screen. The observation fields were selected systematically at random, to avoid any bias in the estimation.

RESULTS

Strain

A continuously decreasing strain gradient ($\Delta\varepsilon_{p_1}/\Delta x$) was observed from the pole to the rim of the stretched blank, and the gradient shape did not change with time. Furthermore, the strain state along any diameter in the blank was always very close to $\varepsilon_{p_1} = \varepsilon_{p_2}$. Consequently, these results may be compared to those obtained with the hydraulic bulging test. Using measurements of

$$\Delta\varepsilon_1^i,\ \Delta\varepsilon_2^i \text{ and } \Delta t^i,$$

where i indicates the deformation step i, the strain history of the stretched blank was estimated from the pole to the rim. Figure 1 shows the evolution of the effective strain as a function of time, measured at the pole and also at distances of 16 mm, 27 mm and 39 mm from the pole. The final effective strains corresponding to each position were 0.95, 0.60, 0.40 and 0.25 respectively. Smoothing the curves $\dot\varepsilon_1 = \Delta\varepsilon_1/\Delta t$, $\dot\varepsilon_2 = \Delta\varepsilon_2/\Delta t$, the effective strain rate values $\dot{\bar\varepsilon}_e$ were calculated using the following equation [2]:

$$\dot{\bar\varepsilon}_e = 2\sqrt{\frac{2+R}{3}}\ \dot\varepsilon_1\ .$$

The calculated $\dot{\bar\varepsilon}_e$ values plotted versus time on Figure 2, correspond to 4 different regions on the blanks, starting from the pole and at distances of 16 mm, 27 mm and 39 mm measured on the fractured blank.

Morphology

The samples deformed in uniaxial tension, plane strain, biaxial strain and the non-deformed sample always had small round cavities or pores and inclusions [8]. Furthermore, the deformed samples had elongated cracks, larger than the round cavities. The use of the scanning electron microscope allowed us to separate the pores, smaller than 1 μm², from the inclusions of the same size. The more frequent inclusions were identified, using the microprobe analyzer [8], as manganese oxisulfides. Flat sections normal to the rolling direction did not show outstanding differences among the three modes of deformation. However, flat sections parallel to the rolling plane had some cracks surrounding inclusions, as shown in Figure 3, especially in the biaxially deformed sample.

Quantitative Analysis

Observing 910 areas on samples corresponding to each deformation mode, it was found that the peculiar morphology shown in Figure 3 was characteristic only of the biaxially stressed sample, its detected frequency in the other modes was negligible: 14.8 features/mm² for $\varepsilon_{p_1} = \varepsilon_{p_2} > 0$, 0.6 features/mm² for $\varepsilon_{p_1} > 0 = \varepsilon_{p_2}$, zero features detected for $\varepsilon_{p_1} > 0 > \varepsilon_{p_2} \simeq \varepsilon_{p_3}$. Five samples were selected, corresponding to effective strain levels measured on the fractured blank of 0.95, 0.60, 0.40, 0.25 and 0 (reference sample represented by +). On each sample 90 areas were observed distributed in three sections normal to the rolling direction.

The features measured at each effective strain level were grouped in 10 classes according to their size (measured in square micrometers) and represented on three different plots. Figure 4 shows the absolute number of cracks and pores Ni, as a function of the class size Ci. To give an estimate of the surface fraction FSi occupied by each class Ci of pores and cracks, the product Ni x Si = FSi, where Si is the mean size of class Ci, was calculated. Plotting this product for each class Ci as a function of class size, Figure 5 was obtained.

The right hand side of Figure 6 shows the absolute number of inclusions Ni (solid line), as a function of the class size Ci; the ordinate of each class, represented by the symbol •, was obtained by analyzing 450 areas, but in order to make this comparable with Figure 4, the results represent the average value for 90 areas. Finally, the left hand ordinates of Figure 6 represent the surface fraction FSi occupied by each class of Ci of inclusions, as a function of the class size. The surface fraction was estimated as indicated above; however each symbol ● now encompasses 5 x 90 areas instead of 90, as was the case in Figures 4 and 5. Furthermore, confidence intervals of one and two standard deviations are also plotted for each class.

DISCUSSION

The measured values of ε_{p_1} and ε_{p_2} at different points of the same blank, obtained at different times, show that the straining is proportional, i.e., $\Delta\varepsilon_1/\Delta\varepsilon_2 = C^t$, throughout the deformation process. Consequently, the metallographic information obtained at different positions when failure is reached (t ∿ 530 seconds on Figure 1), may be considered also to be representative of the history of damage accumulation at the pole of the sample, at different times (points (a), (b), (c) and (d) on Figure 1).

The effective strain rate estimated at the beginning of stretching (t < 250 seconds) has large errors (Figure 2) due to inaccuracy in measuring small deformations; consequently, particular significance should not be attributed to the difference in values of $\dot{\bar\varepsilon}_e$ for different regions of the sample at short times. At longer times, specifically 400 seconds, the differences in $\dot{\bar\varepsilon}_e$ observed probably indicate the beginning of diffuse necking.

The values of $\dot{\bar{\varepsilon}}_e$ observed at the final stages of Figure 2, show that the rate at the pole is approximately 20 times the rate measured at 39 mm from the pole. Such a difference in $\dot{\bar{\varepsilon}}_e$ values may represent a significant contribution to the flow stress, provided that the strain-rate-sensitivity exponent m is positive. Since these differences in strain rate seem to be larger than those obtained in uniaxial tension [9] for the same material, the resistance to instability should be larger in symmetrical biaxial loading. The crack morphology shown in Figure 3 is probably a consequence of the stress state, because it was not detected in uniaxial tension and had a very low frequency of appearance in plane strain experiments.

Figure 4 shows that significant number of defects is already present before stretching the blank. Only larger features are absent in the non-deformed sample: 40 - 70, 70 - 100 and 100 - 400 μm^2. The quantitative distribution of cracks and pores does not include pores that cannot be detected using a magnification of 2600; however, the surface fraction occupied by the smaller pores should be negligible compared to larger sizes (Figure 5). Furthermore, Figure 6 shows that there are no inclusions corresponding to the smaller interval 0.1 - 0.4 μm^2, and very few for the intervals 0.4 - 0.7 and 0.7 - 1.0 μm^2. Consequently, the small cracks and pores have not originated on inclusions, but during the fabrication process.

The shape of the surface fraction distribution of cracks and pores, Figure 5, may arise from super-position of two populations, the first, related to cracks and pores preexisting in the steel, and the second related to the inclusions in the material. Such an assumption is confirmed by the distribution of inclusions in Figure 6, which has only one maximum. The biaxial deformation process seems to increase significantly the number of small pores, as shown in Figure 4, and introduces new larger cracks belonging to the intervals 40 - 70, 70 - 100, 100 - 400 μm^2. Of the remaining classes, the number of pores and cracks does not have significant differences from the non-deformed sample. Figure 5 shows that the increase in surface fraction of damage is only significant in the interval 10 - 40 μm^2. In Figure 5, the interval corresponding to one standard error for effective strain levels of zero and 0.95 is indicated also. The total surface fraction occupied by pores and cracks, and approximate representation of the volume fraction of damage, is estimated by adding all the FSi values of Figure 5 for each strain level. The values found, with the corresponding standard error, are shown in Table 1.

The total amount of damage seems to increase steadily with strain level but, according to the standard deviation values shown in Table 1, the only significant differences lie between the non-deformed state and any deformed strain level.

CONCLUSIONS

1. The stress state has some effect on the morphology of the cracks developed by sheet forming.

2. The quantitative analysis of the size spectrum of damage and inclusions shows that for this specific low carbon rimming steel:

- There is a large number of small cracks and pores, representing a very small area fraction of damage, that is not modified by the deformation process.

- A number of inclusions significantly smaller than the original number of cracks and pores was observed. The size distribution of inclusions is narrower than the size distribution of cracks and pores.
- The larger surface fraction of damage is probably associated with inclusions larger than 10 $(\mu m)^2$. Inclusions smaller than 10 $(\mu m)^2$ do not contribute effectively to the introduction of damage.
- A large amount of damage was already present at an effective strain level of 0.25. Later on, damage increases the size of the cracks, but does not increase the number of large defects significantly.

ACKNOWLEDGEMENTS

The authors acknowledge the support of the "Conselho Nacional de Desenvolvimento Científico e Tecnológico" (GF), and "CEPG" (SLA), and "FINEP".

REFERENCES

1. PAINTER, M. J. and PEARCE, R., 7th Biennial Congress of IDDRG, Amsterdam, October 9 - 13, 1972, Paper 1.
   BROZZO, P., de LUCA, B. and REDINA, R., Ibid, Paper 3.
   FOURDIN, G., JOSSELIN, H. and El HAID, R., Ibid, Paper 15.
2. GHOSH, A. K. and HECKER, S. S., Met. Trans. A., 6, 1975, 1065.
3. MARCINIAK, Z. and KUCZYNSKI, K., Int. J. Mech. Sci., 9, 1967, 609.
4. WILSON, D. V., "Effect of Second Phase Particles on the Mechanical Properties of Steel", I.S.I., London, 1971.
5. DEWSNAP, R. F., PEARCE, R. and BRAUSON, J. R., 7th Biennial Congress of IDDRG, Amsterdam, October 9 - 13, 1972, Paper 12.
6. MOSCA, S. R., de ANDRADE, S. L. and FERRAN, G., Metalurgia, ABM, 32 1976, 733.
7. VEERMAN, C. Chr., 7th Biennial Congress of IDDRG, Amsterdam, October 9 - 13, 1972, Paper 19.
8. de SOUZA, M. C. B. and FERRAN, G., to be published in Metalurgia, ABM.
9. GHOSH, A. K., Met. Trans. A., 5, 1974, 1607.

Table 1 Area Fraction of Damage Introduced as a Function of the Equivalent Strain Level, with the Corresponding Values of the Standard Deviation

Strain Level	Area Fraction of Damage	Standard Deviation
0	2.18×10^{-3}	0.34
.25	5.55×10^{-3}	0.78
.40	5.85×10^{-3}	0.74
.60	6.43×10^{-3}	0.88
.95	8.03×10^{-3}	1.95

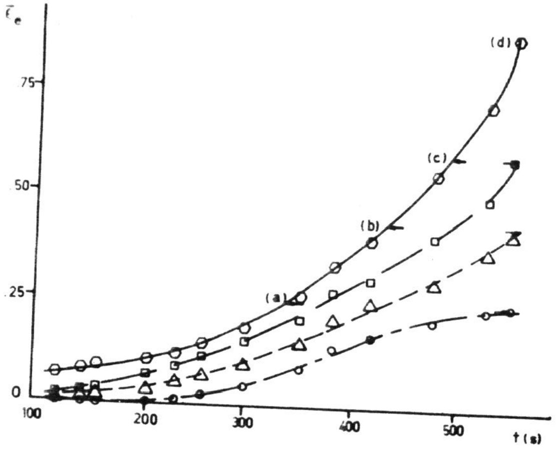

Figure 1 Effective Strain Change versus Time Measured on the Pole (⬡), and at 16 mm (□), 27 mm (Δ) and 39 mm (O) from the Pole, Distances Measured on the Fractured Blank

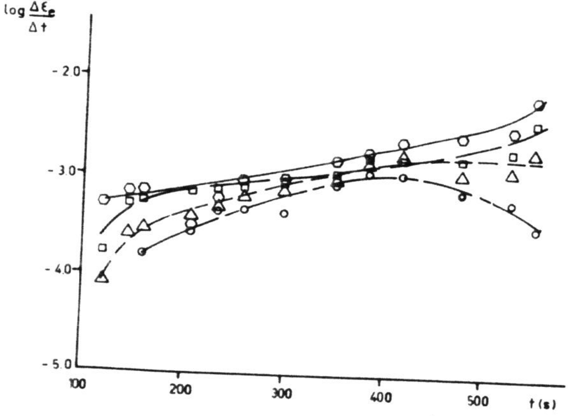

Figure 2 Effective Strain Rate versus Time, on Different Points of the Blank, Symbols as in Figure 1

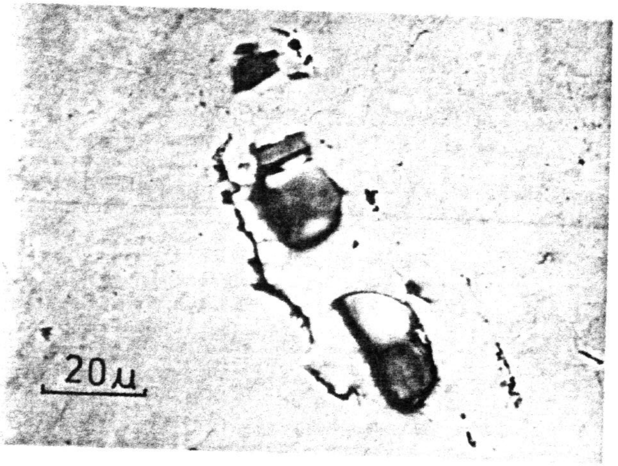

Figure 3 Typical Crack Observed on a Symmetrically Expanded Blank in a Surface Parallel to the Rolling Plane

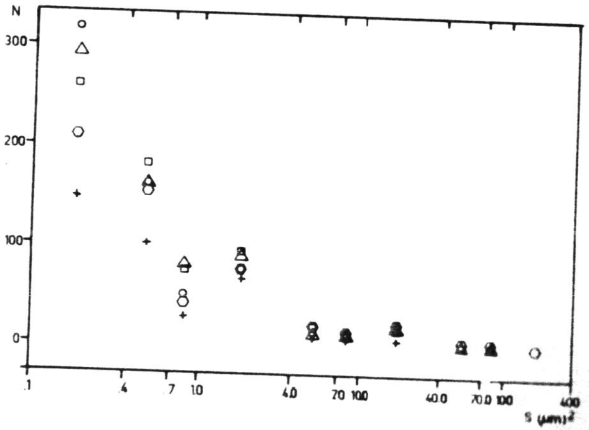

Figure 4 Absolute Number of Pores and Cracks Distributed in Classes. Symbols as in Figure 1, + represents the non-deformed Sample

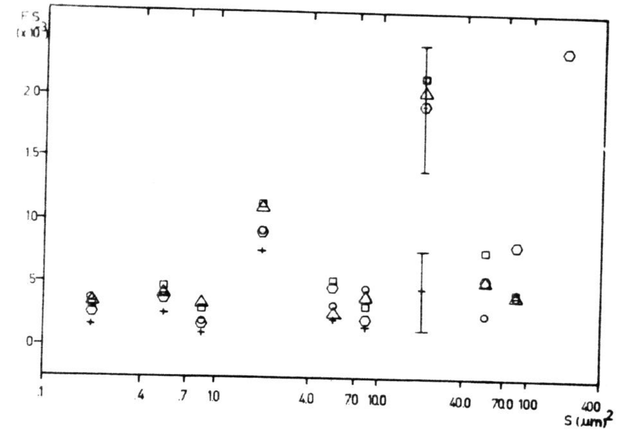

Figure 5 Surface Fraction of Cracks and Pores Distributed in Classes. Symbols as in Figure 4

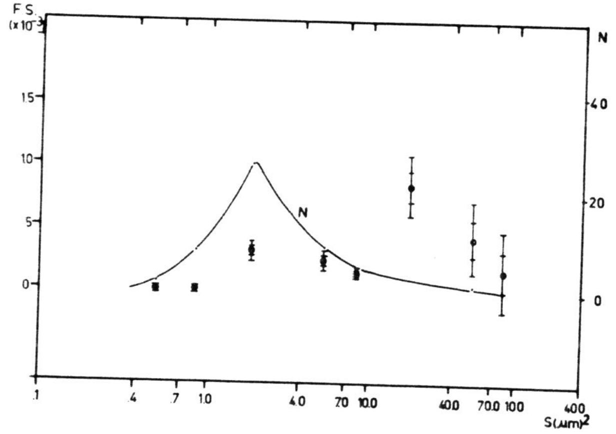

Figure 6 Absolute Number of Inclusions N (Symbol · and Continuous Line Corresponding to the right hand side ordinates) Distributed in Classes. Surface Fraction of Inclusions FS (Symbol ● Corresponding to the left hand side ordinates) Distributed in Classes with Intervals of Confidence of 67% and 95%